Solar Energy Materials & Solar Cells 219 (2021) 110836

Contents lists available at ScienceDirect

Solar Energy Materials and Solar Cells

journal homepage: http://www.elsevier.com/locate/solmat

Breakdown of temperature sensitivity of silicon solar cells by simulation input parameters

Rebekka Eberle *, Andreas Fell, Florian Schindler, Jibran Shahid, Martin C. Schubert

Fraunhofer Institute for Solar Energy Systems ISE, Heidenhofstraße 2, 79110, Freiburg, Germany

A B S T R A C T

As the electrical characteristics of silicon solar cells depend significantly on their temperature T of operation, it is vital to analyze and understand the contributions of the various cell properties in detail in order to optimize silicon solar cells for improved energy output in realistic operation conditions. Within a detailed electro-optical solar cell model, as used for numerical device simulation, accounting for full T-dependence of all cell properties has rarely been attempted to date. This is mainly due to the T-dependence of simulation input parameters not being well known or difficult to measure, resulting in unknown inaccuracy for T-dependent device simulations. This study improves previous T-dependent device models by including the T-dependence of injection-dependent bulk lifetime τ_{bulk} as well as lumped skin surface recombination parameter $J_{0,skin}$, which are commonly assumed T-independent, for the "lumped skin" multidimensional device model employed by the software Quokka3. With this improved T-dependent device model, we present a comprehensive breakdown of a typical PERC cell's temperature sensitivity by each simulation input parameter. As figures of merit we simulate T-coefficients of IV-parameters, as well as energy yields. Overall, we find that the relative influence of the T-dependence of τ_{bulk} and $J_{0,skin}$ is rather small for our examples, clarifying that for modeling typical PERC cells neglecting of their T-dependence does not result in a substantial error. Nonetheless, T-dependency of the bulk material has been found to vary significantly. Also, there remains substantial uncertainty of actual T-dependence of recombination at contacts and lowly doped surfaces worth of further investigations.

1. Introduction

Usually, solar cells are tested and optimized for standard testing conditions (STC) of 25 °C and photon flux density equivalent to 1000 W/m^2 at AM1.5G. The cell's electrical performance substantially decreases with increasing operating temperature, which is typically quantified by a cell's global temperature coefficient. The global temperature dependence of silicon solar cells is already well characterized experimentally, globally as well as locally [1–4]. The dominating effect for the temperature dependence is a decrease of band gap energy E_g with higher temperatures. This mainly causes a reduction in open-circuit voltage V_{OC} due to a rise in the intrinsic charge carrier density n_i resulting in increased recombination rates [1].

An analytical model for the T-dependence of light current-voltage (IV) parameters is given in Ref. [2]: For V_{OC} a linear relation between V_{OC} itself and its temperature coefficient TC_{Voc}, which describes the change of V_{OC} with temperature, is proposed:

$$TC_{V_{OC,rel}} = \frac{1}{V_{OC}}\frac{dV_{OC}}{dT} = -\frac{1}{V_{OC}}\frac{E_{g0} - V_{OC} + \frac{\gamma kT}{q}}{T} \quad (1)$$

In this equation E_{g0} is the extrapolated bandgap voltage at 0 K and γ a free parameter describing the temperature dependency of the cell's dark saturation current density J_0 [2]. γ is commonly fitted to the measured TC_{Voc} and usually has a value between 1 and 4 for high quality cells [2]. Furthermore, due to T-dependent recombination γ can locally reach also negative values in multicrystalline silicon [4].

The reduction of E_g with increasing T further causes a higher absorption of near band gap photons leading to an increase in j_{sc} [2]. Furthermore, the fill factor FF is impacted by the ideal fill factor FF_0 being dependent on the V_{OC}. Additionally, it is influenced by changes of the injection-dependent recombination and the cell's series resistance R_S [3,5]. FF is usually decreasing with increasing temperature as also FF_0 decreases and R_S increases due to higher contact and metal resistance. However, T-dependence of bulk and surface recombination may lead to a non-trivial T-dependence of FF. One can calculate an ideal value for TC_{FF} [1,2], using the ideal fill factor FF_0 without the influence of series resistance R_S as a function of V_{OC}:

$$TC_{FF_{rel}} = \frac{1}{FF}\frac{dFF}{dT} \cong (1 - 1.02\,FF_0)\left[\frac{1}{V_{OC}}\frac{dV_{OC}}{dT} - \frac{1}{T}\right] \quad (2)$$

When employing an electro-optical physical model of the solar cell, e.g. within numerical device simulation or within many characterization methods, T-dependence needs to be considered both for (i) the fundamental material property models, and (ii) for other cell properties like e.

* Corresponding author.
E-mail address: rebekka.eberle@ise.fraunhofer.de (R. Eberle).

https://doi.org/10.1016/j.solmat.2020.110836
Received 8 June 2020; Received in revised form 5 October 2020; Accepted 7 October 2020
Available online 12 October 2020

Table 1
Overview of input parameters for the PERC cell used in the Quokka3 simulations taken from Ref. [15], as well as their *T*-dependence as assumed in this work.

Input parameter	STC value	*TC* in %/K
General geometry		
Cell thickness	170 μm	
Front h-pattern metal grid		
Busbar pitch	31.35 mm (=5 busbars)	
Busbar width	0.8 mm	
Finger pitch	1.5 mm	
Finger width	60 μm	
Optical shading fraction of fingers	0.8	
Finger sheet resistance	0.003 Ω/Ω	0.38 [9]
Contact resistivity	2.7 mΩcm^2	0.91 [8]
Rear full area metal, dashed contacts		
Al metal sheet resistance	17.5 mΩ	
Main contact pitch	1 mm	
Secondary contact pitch	1 mm	
Contact width	72.6 μm	
Contact length	800 μm	
Contact resistivity	3 mΩcm^2	0.91 [8]
Front n + skin		
Sheet resistance	149 Ω	0.1 (simulated)
J_0 non-contacted	31 fA/cm^2	0.5 [11]
J_0 contacted	120 fA/cm^2	0.5 [11]
Collection efficiency T_{ext}	~1	
Texture facet angle	53°	
Average internal reflectance	0.85	
Specular internal reflectance	0.62	
Rear skin		
Sheet resistance	Inf	
J_0 non-contacted	10 fA/cm^2	0.5 [11]
J_0 contacted	400 fA/cm^2	0.5 [11]
Average internal reflectance (contacted, non-contacted)	0.89, 0.98	
Lambertian fraction at rear (contacted, non-contacted)	0.90, 0.66	
Bulk		
Doping density sample i	$7.2{\cdot}10^{15}$ cm^{-3}	
Doping density sample ii	$1.1{\cdot}10^{16}$ cm^{-3}	
Lifetime	See Section 3	See Section 3

g. recombination properties usually being free input parameters into such a solar cell model. Most state-of-the-art solar cell modeling and simulation tools implement well-established models for the *T*-dependence of fundamental material properties. However, the input parameters also have a *T*-dependence, which need to be determined independently to account for in the modeling.

This work uses the multidimensional "lumped skin" modeling approach implemented in the simulation software Quokka3 [6], based on the conductive-boundary model [7]. It is characterized by describing the near-surfaces regions ("skins") effectively by the main lumped input parameters sheet resistance R_{sheet} and recombination property $J_{0,skin}$ as a boundary condition to the multidimensional drift-diffusion model in the bulk. This is in contrast to the physically more detailed description of skins using e.g. doping profile and electron/hole surface recombination velocities as inputs ("detailed skin"). Besides the resulting boost in numerical simplicity and speed, a benefit of the lumped skin approach is the easier experimental determination of the input parameters, which made it a highly popular modeling approach in the PV community.

Table 2
Brief summary of accounting T-sensitivities in studied cases.

Basic Case	Case$_x$	Metallization Case	Full Case
Accounts for *T*-dependence of fundamental material properties only, *T*-dependencies of input parameters neglected	*T*-dependencies of input parameters implemented individually	*T*-dependencies of input parameters except bulk & surface implemented	*T*-dependencies of all input parameters implemented
Input$_{all}$(T) = const.	Input$_x$(T) = see *TC*s in Table 1 Input$_{all-x}$(T) = const.	Input$_{all}$(T) = see *TC*s in Table 1 Input$_{bulk}$(T) = const. Input$_{surf}$(T) = const.	Input$_x$(T) = see *TC*s in Table 1

The required input parameters with potentially significant *T*-dependence into such a lumped skin cell simulation comprise: (i) the bulk lifetime, (ii) the lumped skin properties at the front and rear side, and contacted and passivated regions, respectively, (iii) the specific contact resistivity between the skin and the metal, and (iv) the metal grid resistance towards the measurement pins or cell interconnectors, commonly defined by an external series resistance.

While values for the *T*-dependence for (iii) and (iv) exists [8,9] or can be measured with moderate effort, considering the *T*-dependence of the bulk lifetime τ_{bulk} and of the lumped skin properties was not attempted so far, due to being experimentally not easily accessible. In this work we include those effects by using measurements recently described [4,10,11]. For an exemplary typical PERC cell we perform *T*-dependent Quokka3 simulations accounting for the best-known *T*-dependence of all simulation input parameters. Furthermore, the cell simulation results are fed into a yield modeling described in Ref. [12–14] for two locations with different climate. This results in a breakdown of the *T*-sensitivity of IV-parameters and yield by all simulation input parameters to clarify their relative influence.

1.1. Device simulation in quokka3

The device simulation is based on an industrial silicon PERC cell corresponding to an industrial standard in 2018, details for this simulation at STC are described in Ref. [15] and shown in Table 1.

Quokka3 employs up-to-date models for *T*-dependent fundamental silicon properties, namely the band-gap [16], intrinsic charge carrier density [17], band-to-band absorption coefficient [18] and mobility [19,20]. It thereby automatically accounts for the main *T*-dependent effects.

For determining the *T*-dependence of the generation under AM1.5g spectrum, the so called "Text-Z" model of Quokka3 is used which uses the *T*-independent spectral input parameters surface transmission T_{ext} and path length enhancement *Z* as shown in Ref. [21]. In the PERC cell of this work, *Z* is calculated from the internal optical properties of the skin (see details in Ref. [15]), which can also assumed *T*-independent to produce a *T*-independent *Z*.

An overview of the electrical input parameters is given in Table 1. From the properties given in Ref. [15], we only change the bulk properties to our own bulk lifetime measurements of two wafers representative for PERC cells, to include a measured *T*-dependence of the injection-dependent bulk lifetime, see Section 3 for details. Notably, also the bulk resistivity has been adjusted to correspond to the respective lifetime sample (see Fig. 3 in Ref. [15]).

Amongst the electrical input parameters special attention needs to be paid to the lumped skin recombination parameter $J_{0,skin}$: a value for $J_{0,skin}$ should actually always be accompanied by a value of the intrinsic charge carrier density n_i assumed during its determination, as the quotient $J_{0,skin}/n_i^2$ is the actual parameter determined by $J_{0,skin}$ measurement techniques. This is even more important to consider when investigating *T*-dependence, as it is well known that $J_{0,skin}$ varies largely with temperature being dominantly caused by the change of n_i, while J_0/n_i^2 can be considered *T*-independent as a first approximation. Notably this is the default assumption in Quokka3, meaning that for any $J_{0,skin}$ input parameter not the value of the parameter, but the quotient J_0/n_i^2 is held constant when changing the device temperature. Only recently the validity of this assumption was tested experimentally for typical diffused junctions [11], where a moderate *T*-dependence of J_0/n_i^2 was found to be

~0.5%/K for all investigated passivated junctions, while a larger and apparently random spread from ~0.5%/K to ~1.5%/K was observed for metallized junctions. For simplicity, we also apply 0.5%/K to metallized (i.e. contacted) skin regions, but note that a substantial uncertainty still exists for the *T*-dependence of contact recombination. This parametrization was gained on FZ silicon but is still valid for CZ silicon with low defect density as it the bulk defects have little impact of the $J_{0,skin}$ of diffused junctions.

R_{sh} is assumed to increase minor by 0.1%/K which is determined by simulations in Quokka3 using standard industrial diffusion profiles. The *T*-dependence of contact resistivity is taken from Ref. [8], for the change of finger resistivity with temperature the literature value for pure silver as 0.38%/K is chosen [9]. Note that the selection of the upper temperature for simulation other than STC is not crucial as in the temperature range of operation of solar cells all parameters seem to behave in a linear manner.

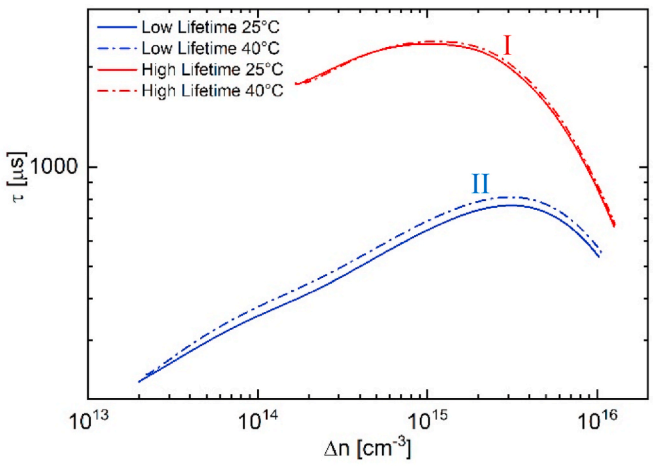

Fig. 1. Lifetime τ_{bulk} obtained from modulated PL measurements [22] for two monocrystalline lifetime samples processed according to PERC cells with all relevant high temperature steps. Due to different material quality lifetimes τ at 25 °C differ significantly.

The procedure used for calculation of temperature coefficients of V_{OC}, *FF*, j_{SC} and η for different cases is explained in the following, Table 2 describes the investigated cases briefly. Light IV-curve simulations are performed at a device temperature of 25 °C and one higher temperature (namely 40 °C). The temperature coefficients *TC* for V_{OC} (TC_{Voc}), *FF* (TC_{FF}), j_{SC} (TC_{jsc}) and η (TC_{η}) are then calculated by assuming a linear change of these parameters with temperature in the studied temperature range.

For the basic case, the input parameters are not adjusted at the higher temperature kept at their value at STC, meaning that the *T*-dependence of the cell solely results from the *T*-dependence of the fundamental material properties. Note that the basic case is idealized but likely not a common case, as the *T*-dependence of the metallization could routinely be taken into account by a measured *T*-dependence of the series resistance. The inclusion of the *T*-dependence of only those metallization related inputs is thus called the metallization case which still neglects the *T*-dependence of bulk and skin recombination. The full case means that all input parameters are adjusted at the higher simulation temperature according the T-dependence given in Table 1. Consequently, the differences between the metallization case and full case quantify an improvement of *T*-dependent cell modeling of this work compared to previous works.

To breakdown the influence of each individual input parameter on the cell's *T*-dependence, further cases are simulated which consider the *T*-dependence of only one input parameter at a time.

As a final step, the impact of *T*-dependent input parameters for feeding the device simulation results into an energy yield prediction is studied. For this, the yearly energy yield at two locations with very different climatic conditions is calculated via SmartCalc.CTM [12,13] assuming a standard 60 cell module [12]. SmartCalc.CTM is a tool for

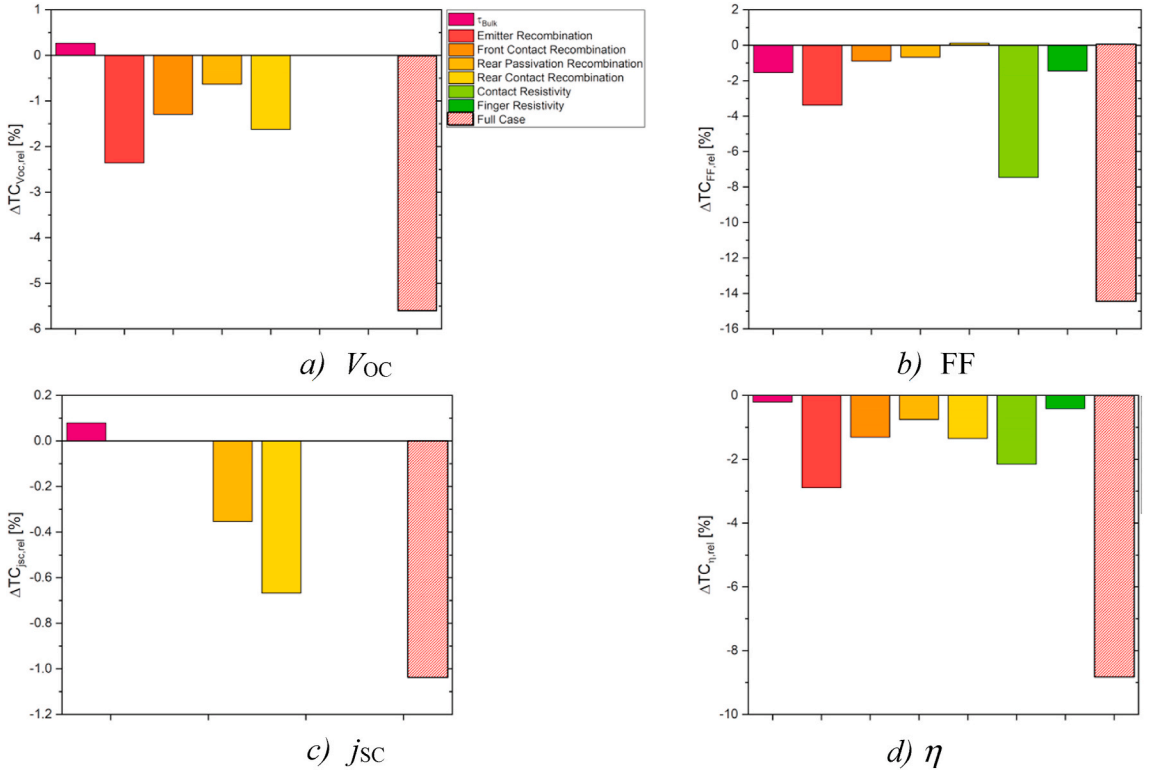

Fig. 2. Relative deviation of *TC* from basic case simulation for implementation of each input parameter's temperature dependence as well as combined implementation using lifetime of PERC lifetime sample I a) for TC_{Voc}, b) TC_{FF}, c) $TC_{jsc,}$ and d) TC_{η}.

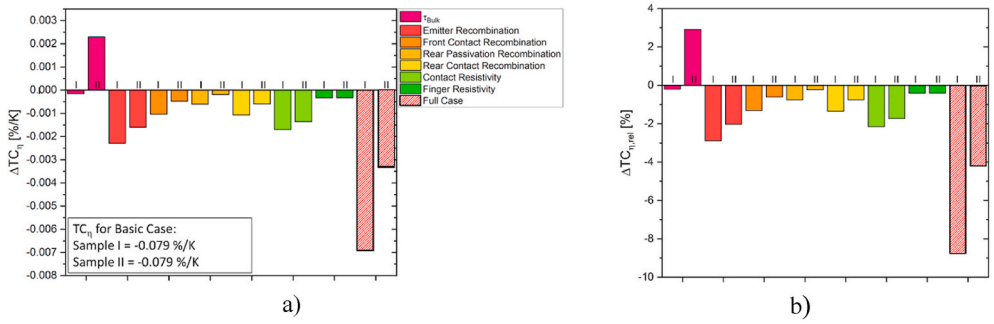

Fig. 3. a) Absolute as well as b) relative deviation from *TC* for implementation of each input parameter's temperature dependence as well as combined implementation to basic case simulation using lifetimes of two different PERC lifetime samples TC_η. The numbers in the graphs correspond to both lifetime samples I and II.

predicting module power and efficiency from material as well as geometric data for cell, interconnection and module designs and calculates cell-to-module (CTM) losses. The methodology, which is used by the tool, analyzes photovoltaic inactive module areas and optical effects like reflection, absorption as well as electrical losses induced by cell interconnection. It is further able to do yield calculations for a specific set of module and weather data. We use weather data gathered at the locations of Norwich, United Kingdom, and Rafah, Egypt, which represent very diverse climate and irradiation conditions with low and high average temperatures respectively (data gained by Fraunhofer ISE). To compare the different locations, the normalized energy yield is used as the figure of merit, which is a common more easily comparable metric defined as the energy yield per installed capacity [kWh/kW_{peak}].

2. Results

2.1. Bulk lifetime measurement

Two different quality bulk materials were chosen to analyze the influence of bulk quality on temperature dependence. The injection-dependent bulk lifetime τ_{bulk} of two lifetime samples typical for PERC cells made of 1 Ωcm p-type CZ silicon is measured via modulated photoluminescence (mod-PL) [22] at STC temperature of 25 °C as well as at 40 °C. The samples with a thickness of 180 μm are symmetrically passivated with Al_2O_3. All high temperature steps typical for the production of PERC cells were conducted to achieve a τ_{bulk} representative for a final cell. Fig. 1 provides an overview of the injection-dependent τ_{bulk}, which was measured for the analyzed samples at 25 °C and 40 °C. Sample II shows an overall decreased lifetime level compared to Sample I, for both samples τ_{bulk} decreases at high injection density.

2.2. Temperature sensitivity of IV-Parameters

2.2.1. General implications by implementing T-sensitivity

To assess the impact of implementing more detailed *T*-dependence on simulated temperature coefficients, the absolute and relative deviation between the basic case and all other simulated cases is calculated. The absolute as well as relative deviations of the *TC*s compared to the basic case are shown in Fig. 2 and are calculated by as

$$\Delta TC_{X,abs} = TC_X - TC_{Basic\ Case} \text{ and } \Delta TC_{X,rel} = \frac{\Delta TC_{X,abs}}{|TC_{X,abs}|}. \quad (3)$$

We first focus on the results for the high lifetime sample (see Fig. 1, lifetime curve of Sample I). For TC_{Voc} (Fig. 2 a)), the strongest deviation to the basic case is caused by the emitter recombination. Overall, recombination in the emitter limits the V_{OC} detrimentally, at STC as well as higher *T*, and, due to the *T*-dependence of intrinsic carrier density $n_{i,eff}$, strongly increases with temperature. Front and rear contact passivation use the same *TC* of $J_{0,skin}/n^2_{i,eff}$, and cause a further decrease of TC_{Voc} compared to the basic case. The combined effect of including each input parameter's *TC* in the full case leads to a decrease of combined TC_{Voc} of up to −0.11 mV/K (5.5% relative change).

TC_{FF} in Fig. 2 b) is dominated by the *T*-dependence of the contact resistivity which dominates the series resistance R_S. The deviation of the full to the basic case is −0.012%/K (14.4% relative change).

For TC_{jsc}, we observe the largest changes compared to the basic case by considering the *TC* of recombination at the rear (passivation and contact). Compared to the changes in TC_{Voc} and TC_{FF}, ΔTC_{jsc} between basic and full case is small (−0.00017 mA/(cm^{2}K) absolute and 1.0% relative change).

Lastly, Fig. 2 d) illustrates the combined effect of the analyzed IV parameters' *TC* deviations in Fig. 2 a) to Fig. 2 c) on ΔTC_η. The combined impact results in an absolute deviation ΔTC_η of −0.007%/K (9% relative change).

2.3. Effect of τ_{bulk} & its T-dependence

All the previous results were gathered by using the *T*-dependent lifetime of the high quality lifetime sample. Next, we show the same analysis for a sample featuring significantly lower bulk lifetime. The respective τ_{bulk} of this Sample II is also shown in Fig. 1 having an overall lower lifetime level than Sample I and differing injection dependence as well as stronger *T*-dependence.

Results for simulations using different lifetime input are shown in

Table 3
Overview of IV parameters for Sample I and II, simulated performance at 25 °C and 70 °C for basic case as well as for full case and the case without temperature dependence of bulk and surface is listed. Assessment of analytical model for TC_{FF}.

Sample	Cell Parameter	@25 °C	Basic Case @70 °C	Metallization Case @70 °C	Full Case @70 °C
I	V_{OC}	685.6 mV	595.1 mV	595.0 mV	590.1 mV
	FF	81.7%	77.8%	77.5%	77.3%
	j_{SC}	39.77 mA/cm^2	40.53 mA/cm^2	40.53 mA/cm^2	40.52 mA/cm^2
	η	22.3%	18.74%	18.63%	18.41%
II	V_{OC}	683.0 mV	592.3 mV	592.4 mV	588.4 mV
	FF	81.2%	77.2%	76.9%	77.1%
	j_{SC}	39.62 mA/cm^2	40.37 mA/cm^2	40.37 mA/cm^2	40.37 mA/cm^2
	η	22.0%	18.45%	18.34%	18.26%

Table 4
Comparison of simulated *TC*s and *TC*s calculated from analytical model by Green [1].

Sample	V_{oc} @ 25 °C	$TC_{Voc,rel}$	γ	Simulated $TC_{FF,rel}$	Analytical $TC_{FF,rel}$
		Basic/Full Case	Basic/ Full Case	Basic/Full Case	Basic/Full Case
I	685.6 mV	−0.293%/ K/-0.310%/K	6.43/ 7.72	−0.107%/ K/-0.120%/K	−0.044%/K/-0.045%/K
II	683.0 mV	−0.295%/ K/-0.308%/K	6.38/ 7.39	−0.109%/ K/-0.112%/K	−0.044%/K/-0.045%/K

Fig. 3, which illustrates the absolute (Fig. 3 a)) as well as relative deviation (Fig. 3 b)) in TC_η of all cases to the basic case. At a first glance it is obvious that varying τ_{bulk} leads to different simulated *T*-sensitivities, and hence, varying ΔTC_η for all simulated cases. The strongest effect is induced by the *T*-dependence of τ_{bulk}, which may vary substantially depending on the specific material as shown by an opposite deviation in Fig. 3a) and b). The common trend of lower efficiency correlating with increased *T*-sensitivity is true for the two investigated samples only in the basic case. It is a notable curiosity for the more realistic full case that TC_η for the low quality Sample II becomes lower than for the high quality Sample I.

Table 3 provides an overview of simulated IV parameters for both lifetime samples for STC and for a high operating temperature of 70 °C. As already stated, the lower level of τ_{bulk} of Sample II results in decreased IV parameters compared to Sample I. When the basic and full case are compared at 70 °C, the neglecting of all input parameters' *T*-dependence results in an error in efficiency η of 0.2–0.3%. However, this error approximately halves for the more common metallization case which considers the *T*-dependence of the metallization inputs, but still neglects *T*-dependence of bulk and surface recombination.

Using the theoretical parametrizations of TC_{Voc} and TC_{FF}, as was shown in Eq. (1) and Eq. (2), the usefulness of the analytical TC_{FF} is analyzed by the deviation between analytical and simulated TC_{FF}. Via Eq. (2) and applying V_{oc} at STC and TC_{Voc} of the basic and full case, analytical TC_{FF} is calculated and compared with the respective simulated TC_{FF}. An overview is given in Table 4. When the analytical TC_{FF} is compared to the simulated TC_{FF}, there is a deviation of more than 50% regardless of the sample type and for both cases. This clarifies that neglecting of the *T*-dependence of R_S in the analytical calculations for TC_{FF} is generally not the dominant reason for the commonly observed mismatch between the analytical and experimentally observed TC_{FF}.

2.4. Impact on energy yield

How the different cases' *TC*s influence the simulation of yearly energy output is depicted in Table 5 and Fig. 4 for both studied locations. For both locations there is an influence of the different cases on the calculated energy yield as the temperature coefficients of IV parameters deviate from the basic case. In Fig. 4 the breakdown of the influence of the input parameter's *T*-dependence on the normalized energy yield are plotted for a) Norwich and b) Rafah in the same manner as for the previous graphs in section 4.1. As can be seen in Table 5, the difference

Table 5
Predicted normalized energy yield for locations of Norwich, United Kingdom, and Rafah, Egypt, for basic and full case using different lifetime input.

	Sample	Basic Case	Full Case
$Yield_{Norwich}$	I	820 kW h/kWp	822 kW h/kWp
	II	829 kW h/kWp	830 kW h/kWp
$Yield_{Rafah}$	I	1700 kW h/kWp	1696 kW h/kWp
	II	1711 kW h/kWp	1708 kW h/kWp

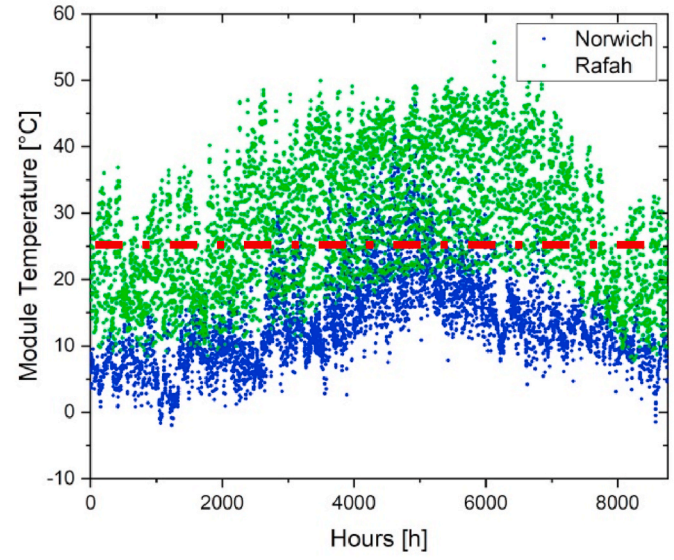

Fig. 5. Simulated hourly module temperature for module operating in Norwich and Rafah, the STC temperature of 25 °C is marked.

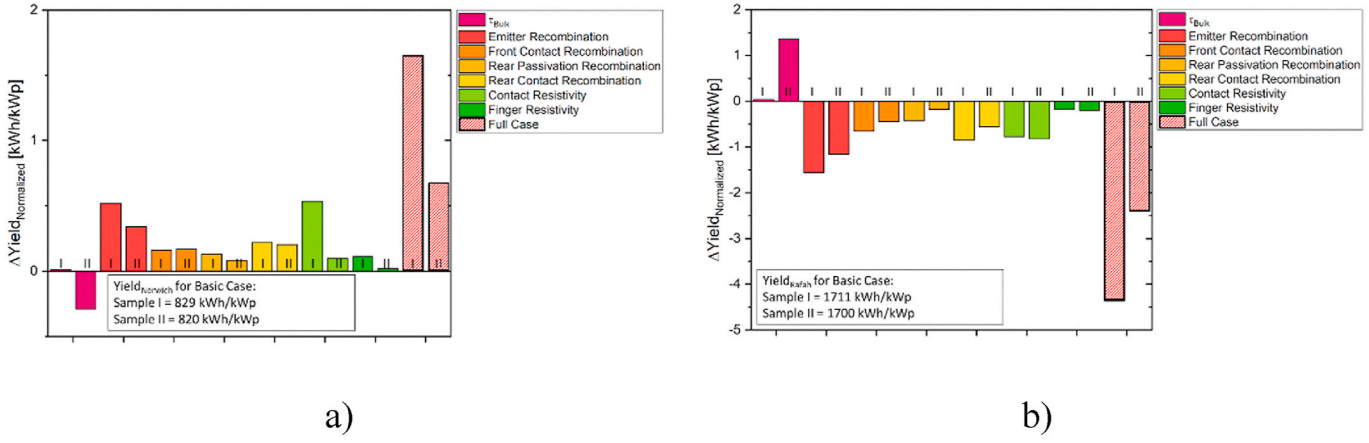

Fig. 4. Difference to basic case in normalized yearly energy yield for silicon solar module placed in a) Norwich and b) Rafah. (For interpretation of the references to colour in this figure legend, the reader is referred to the Web version of this article.)

in normalized energy yield for both locations between the basic and full case is less than 0.2%. Interestingly, the trends for Norwich and Rafah appear to be opposing each other: For simulations of Sample I and Sample II a higher normalized energy yield is predicted for the full case for Norwich, while for Rafah exactly the opposite is true. This behavior can be explained by the operating module temperatures, which are shown in Fig. 5 for both locations. At Rafah the higher outdoor temperature and incident irradiation leads to an average module temperature higher than STC. As in the full case TC_η is increased in absolute values compared to the basic case, an increase in temperature results in lower energy yield. Due to low outdoor temperature and rather low average irradiation intensity, the operating module temperature in Norwich is on average lower than STC, which explains the increase in predicted yearly energy yield. Nevertheless, the observed effect on energy yield prediction is small clarifying that the typical simplified approaches do not suffer from a significant systematic inaccuracy.

Furthermore, when the relative bar heights of Fig. 4a) and b) are compared with Fig. 3 b), illustrating deviation of TC_η, it can be seen that the relative impact of the individual input parameters on energy yield closely correlates to the respective impact on TC_η. This confirms an intuitive expectation: an input parameter's impact on TC_η approximately determines its impact on energy yield.

3. Conclusion

In this work we increased the understanding of a silicon solar cell's temperature sensitivity by presenting its breakdown by all relevant input parameters for the "lumped skin" model of Quokka3. Measured T-dependencies of injection-dependent bulk lifetime τ_{bulk} as well as lumped skin surface recombination parameter $J_{0,skin}$, previously assumed to be independent of temperature, were accounted for in addition to the T-dependence of contact metal grid resistance, which results in lower cell performance at increased temperature. The error when assuming temperature independence of bulk and surface properties is quantified to be a small effect in the range of several percent. Some substantial uncertainty for a general conclusion on the influence exists with the T-dependence of the bulk lifetime, which has the largest individual impact and varies substantially for the two investigated samples, as well as of contact recombination.

For our studied examples, we have further shown that the influence of the T-dependence of the input parameters on the subsequent prediction of energy yield at varying locations of operation is rather small (« 1%). As would be intuitively expected, the yield breakdown was shown to closely correlate with the breakdown of TC_η.

CRediT authorship contribution statement

Rebekka Eberle: Conceptualization, Methodology, Investigation, Writing - original draft, Writing - review & editing, Visualization, Project administration. **Andreas Fell:** Software, Writing - review & editing, Validation. **Florian Schindler:** Supervision. **Jibran Shahid:** Investigation. **Martin C. Schubert:** Supervision, Funding acquisition.

Declaration of competing interest

The authors declare that they have no known competing financial interests or personal relationships that could have appeared to influence the work reported in this paper.

Acknowledgement

We thank Christian Reise for providing weather data for energy yield prediction. This work was supported by the Bundesministerium für Wirtschaft und Energie BMWi and by industry partners within the research project PROGNOSIS under contract No. 0324160. Rebekka Eberle would like to thank the "Studienstiftung des deutschen Volkes" for funding her dissertation project. The authors are responsible for the content.

References

[1] M.A. Green, General temperature dependence of solar cell performance and implications for device modelling, Prog. Photovoltaics Res. Appl. 11 (2003) 333–340, https://doi.org/10.1002/pip.496.
[2] M.A. Green, K. Emery, A.W. Blakers, Silicon solar cells with reduced temperature sensitivity, Electron. Lett. 18 (1982) 97, https://doi.org/10.1049/el:19820066.
[3] O. Dupre, R. Vaillon, M.A. Green, Experimental assessment of temperature coefficient theories for silicon solar cells. IEEE 42nd Photovoltaic Specialist Conference (PVSC), IEEE, New Orleans, LA, 2015, pp. 1–3.
[4] R. Eberle, A. Fell, S. Mägdefessel, F. Schindler, M.C. Schubert, Prediction of local temperature-dependent performance of silicon solar cells, Prog. Photovoltaics Res. Appl. 27 (2019) 999–1006, https://doi.org/10.1002/pip.3130.
[5] A. Martin, Green, Silicon Solar Cells: Advanced Principles & Practice, Centre for Photovoltaics devises and systems, University of New South Wales, Sydney, 1995.
[6] A. Fell, J. Schön, M.C. Schubert, S.W. Glunz, The concept of skins for silicon solar cell modeling, Sol. Energy Mater. Sol. Cell. 173 (2017) 128–133, https://doi.org/10.1016/j.solmat.2017.05.012.
[7] R. Brendel, Modeling solar cells with the dopant-diffused layers treated as conductive boundaries, Prog. Photovoltaics Res. Appl. 20 (2012) 31–43, https://doi.org/10.1002/pip.954.
[8] R. Hönig, Evaluation and Microstructure Analysis of Thick Film Contacts for Industrial Silicon Solar Cells, University Freiburg, Freiburg, 2014.
[9] R.A. Serway, J.W. Jewett JR., Principles of Physics, Secondnd, Fort Worth Saunders College Pub, 1998.
[10] R. Eberle, A. Fell, T. Niewelt, F. Schindler, M.C. Schubert, Analysis of temperature dependent surface recombination properties, in: AIP Conference Proceedings, 2019, p. 140001.
[11] R. Eberle, A. Fell, A. Richter, T. Niewelt, F. Schindler, M.C. Schubert, Analysis of temperature dependent characteristics of diffused regions in silicon solar cells, in: IEEE 46th Phtotovoltaic Specialists Conference, 2019, pp. 3032–3036.
[12] M. Mittag, C. Kutter, S. Hoffmann, P. Romer, A.J. Beinert, T. Zech, Electrical and Thermal Modeling of Junction Boxes, Proceedings of 33rd EUPVSEC, Amsterdam, The Netherlands, 2017.
[13] M. Mittag, A. Pfreundt, J. Shahid, N. Wöhrle, H.D. Neuhaus, Techno-economic analysis of half cell modules: the impact of half cells on module power and costs. Proceedings of 36th European Photovoltaic Solar Energy Conference and Exhibition, EU PVSEC), Marseille, France, 2019.
[14] J. Shahid, M. Mittag, M. Heinrich, A multidimensional optimization approach to improve module efficiency, power and costs. Proceedings of the 35th European Photovoltaic Solar Energy Conference and Exhibition, EU PVSEC), Brussels, Belgium, 2018.
[15] A. Fell, P.P. Altermatt, A detailed full-cell model of a 2018 commercial PERC solar cell in Quokka3, IEEE J. Photovoltaics 8 (2018) 1443–1448, https://doi.org/10.1109/JPHOTOV.2018.2863548.
[16] R. Pässler, Dispersion-related description of temperature dependencies of band gaps in semiconductors, Phys. Rev. B 66 (2002), https://doi.org/10.1103/PhysRevB.66.085201.
[17] R. Couderc, M. Amara, M. Lemiti, Reassessment of the intrinsic carrier density temperature dependence in crystalline silicon, J. Appl. Phys. 115 (2014) 93705, https://doi.org/10.1063/1.4867776.
[18] C. Schinke, P. Christian Peest, J. Schmidt, R. Brendel, K. Bothe, M.R. Vogt, I. Kröger, S. Winter, A. Schirmacher, S. Lim, H.T. Nguyen, D. Macdonald, Uncertainty analysis for the coefficient of band-to-band absorption of crystalline silicon, AIP Adv. 5 (2015) 67168, https://doi.org/10.1063/1.4923379.
[19] D.B.M. Klaassen, A unified mobility model for device simulation—II. Temperature dependence of carrier mobility and lifetime, Solid State Electron. 35 (1992) 961–967.
[20] D.B.M. Klaassen, A unified mobility model for device simulation—I. Model equations and concentration dependence, Solid State Electron. 35 (1992) 953–959, https://doi.org/10.1016/0038-1101(92)90325-7.
[21] A. Fell, K.R. McIntosh, K.C. Fong, Simplified device simulation of silicon solar cells using a lumped parameter optical model, IEEE J. Photovoltaics 6 (2016) 611–616, https://doi.org/10.1109/JPHOTOV.2016.2528407.
[22] J.A. Giesecke, M.C. Schubert, B. Michl, F. Schindler, W. Warta, Minority carrier lifetime imaging of silicon wafers calibrated by quasi-steady-state photoluminescence, Sol. Energy Mater. Sol. Cell. 95 (2011) 1011–1018, https://doi.org/10.1016/j.solmat.2010.12.016.